



UvA-DARE (Digital Academic Repository)

Quantitative and localized spectroscopy for non-invasive bilirubinometry in neonates

Bosschaart, N.

Publication date
2012

[Link to publication](#)

Citation for published version (APA):

Bosschaart, N. (2012). *Quantitative and localized spectroscopy for non-invasive bilirubinometry in neonates*. [Thesis, fully internal, Universiteit van Amsterdam].

General rights

It is not permitted to download or to forward/distribute the text or part of it without the consent of the author(s) and/or copyright holder(s), other than for strictly personal, individual use, unless the work is under an open content license (like Creative Commons).

Disclaimer/Complaints regulations

If you believe that digital publication of certain material infringes any of your rights or (privacy) interests, please let the Library know, stating your reasons. In case of a legitimate complaint, the Library will make the material inaccessible and/or remove it from the website. Please Ask the Library: <https://uba.uva.nl/en/contact>, or a letter to: Library of the University of Amsterdam, Secretariat, P.O. Box 19185, 1000 GD Amsterdam, The Netherlands. You will be contacted as soon as possible.

CHAPTER 4

Quantitative measurements of absorption spectra in scattering media by low-coherence spectroscopy

Low Coherence Spectroscopy (LCS) is a novel spectroscopic method that allows for quantitative and localized assessment of absorption spectra by combining reflection spectroscopy with low coherence interferometry. We describe absorption coefficient (μ_a) measurements by LCS in tissue simulating phantoms with varying scattering and absorbing properties. We used LCS in the 455–680 nm wavelength range with a spectral resolution of 8 nm to obtain μ_a spectra with $\pm 0.5 \text{ mm}^{-1}$ accuracy. We conclude that LCS is a promising technique for the *in vivo* determination of tissue chromophore concentrations.

Part of this work has been published in: N. Bosschaart, M.C.G. Aalders, D.J. Faber, J.J.A. Weda, M.J.C. van Gemert and T.G. van Leeuwen, "Quantitative measurements of absorption spectra in scattering media by low-coherence spectroscopy", *Optics Letters* 34(23), 3746-3748 (2009)

4.1 Introduction

Optical spectroscopy for *in vivo* determination of chromophore concentrations (e.g. hemoglobin and bilirubin) offers an alternative to frequent and invasive drawing of blood followed by time consuming laboratory analysis. However, due to lack of knowledge of the optical path in tissue, the current clinically applied spectroscopic techniques such as elastic scattering, absorption and differential path length spectroscopy [1-3] depend on photon path length models for the determination of absolute chromophore concentrations. Another limitation is the lack of localization [1,2], i.e. the measured signal originates from a large volume, which makes it difficult to confine the measurement to a preferred target volume such as the microcirculation in the skin. *Quantitative* (i.e. absolute concentrations) and localized spectroscopic measurements of tissue chromophores require knowledge of (or control over) the path length of light in tissue, because then tissue absorption coefficients, which are directly related to chromophore concentrations, can be calculated using Beer's law.

In this Chapter, we demonstrate for the first time that low-coherence spectroscopy (LCS) allows for quantitative assessment of absorption spectra in scattering media as a first step toward non-invasive *in vivo* tissue chromophore concentration measurements. LCS combines reflection spectroscopy with low coherence interferometry (LCI) to control the path length of the detected light. To validate this method, we performed *in vitro* measurements of absorption coefficient spectra on samples with known absorption and scattering properties.

LCS is a novel extension of LCI and can therefore be placed alongside techniques such as optical coherence tomography (OCT) and path length resolved optical Doppler measurements [4]. LCS recovers spectroscopic information at controlled path lengths from the sample, similar to spectroscopic OCT (sOCT) [5-8]. However, LCS is fully optimized for spectroscopy, instead of tomography. This allows a system design with high spectral resolution at the sacrifice of spatial resolution. Also, sampling intervals can be optimized for spectroscopic purposes and the measurement volume can be enlarged for better signal to noise ratios. Our LCS system operates in the visible wavelength range, because of the distinct features of important chromophores such as bilirubin and hemoglobin in this region, compared to the near infrared region (NIR). Hence, chromophore concentration alterations induce more pronounced changes in absorption. In sOCT, spectroscopy is combined with imaging, which limits the available wavelengths to the NIR to obtain sufficient imaging depth. Other path length resolved spectroscopic methods, such as time of flight [9] and phase resolved spectroscopy [10] measure the optical path length, rather than controlling it. In addition, their range of validity is limited to large path lengths, which compromises localization.

4.2 Theory

The LCS system described in this thesis is based on a Michelson interferometer (Figure 4.1). Low-coherent light originating from the source is divided by a beam splitter into a sample arm and a reference arm, with lengths x_s and x_r , respectively. Back scattering of photons by the sample in the sample arm results in a sample arm field E_s , and back

reflection of photons by a mirror in the reference arm results in a reference arm field E_R . Both fields recombine at the beam splitter and are guided towards a photo detector, where they interfere.

The photo detector current i_D is proportional to the square of the optical field at the detector E_D^2 :

$$i_D \propto \langle |E_D|^2 \rangle \propto \langle |E_S + E_R|^2 \rangle \propto \langle |E_S|^2 + |E_R|^2 + 2E_S E_R \rangle \quad (4.1)$$

in which the triangular brackets denote integration over the detector response time. The latter part of this expression, $2E_S E_R$, denotes the interferometric portion of the signal, i.e. the AC part of the detector current:

$$i_{AC} \propto \langle 2E_S E_R \rangle \quad (4.2)$$

This interferometric signal is directly related to the time (t) dependent optical path length difference between the sample arm and the reference arm, $\Delta L(t) = 2(x_S(t) - x_R(t))$. In the case of a monochromatic light source, $i_{AC}(t)$ can be described by:

$$i_{AC}(t) \propto 2\sqrt{I_S(\Delta L(t)) \cdot I_R} \cdot \cos(k \cdot \Delta L(t)) \quad (4.3a)$$

where I_S and I_R are the signal intensities in the sample and reference arm, respectively, and k is the wavenumber ($k=2\pi/\lambda$, with wavelength λ) [11].

In the case of a broad band, or low-coherent light source, $i_{AC}(t)$ is integrated over the source spectrum:

$$i_{AC}(t) \propto 2 \int \sqrt{I_S(k, \Delta L(t)) \cdot I_R(k)} \cdot \cos(k \cdot \Delta L(t)) \cdot dk = \sqrt{I_S(\Delta L(t)) \cdot I_R} \cdot \cos(k_0 \cdot \Delta L(t)) \quad (4.3b)$$

in which k_0 is the center wave number of the source spectrum. As a consequence, interference between E_S and E_R can only be observed within the coherence length l_c of the source, which is the limiting axial resolution at which $i_{AC}(t)$ can be acquired (assuming a Gaussian shaped source spectrum):

$$l_c = \frac{2 \ln 2}{\pi} \frac{\lambda_0^2}{\lambda_{FWHM}} \quad (4.4)$$

with λ_0 the center wavelength of the source spectrum and λ_{FWHM} the bandwidth, or full width at half maximum (FWHM) of the source spectrum [11].

The broad bandwidth of a low-coherent source can be used for spectroscopic purposes, which is the basic principle of LCS. Hence, we are interested in the frequency content (which is related to wavelength in LCS) of the signal i_{AC} . Therefore, we regard the power spectrum $S(f)$ of $i_{AC}(t)$, obtained by Fourier transformation of $i_{AC}(t)$:

$$S(\lambda) : \Leftrightarrow S(f) = \left| \mathfrak{F}\{i_{AC}(t)\} \right|^2 \quad (4.5)$$

In the remaining part of this Chapter, all wavelength dependent parameters will be indicated by a bold faced character, e.g $\mathbf{S} = S(\lambda)$.

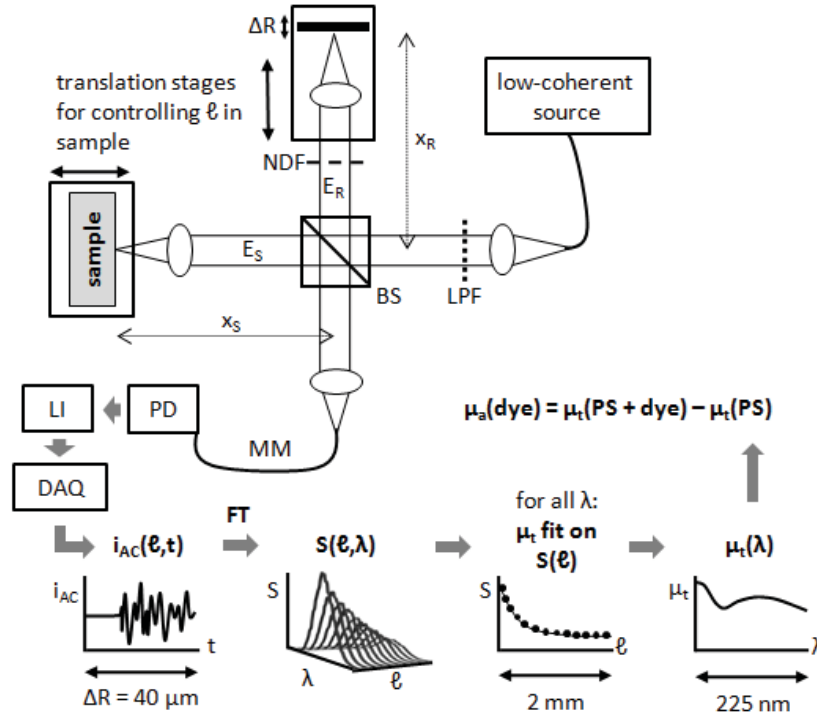


Figure 4.1 The LCS system (upper part) and a schematic overview of the signal processing (lower part). E_s/E_r : optical field in sample/reference arm, x_s/x_r : length of sample/reference arm, LPF: low pass filter, BS: beam splitter, NDF: neutral density filter, ΔR : scanning range of the piezo driven reference mirror, MM: multimode graded index detection fiber, PD: photo diode, LI: lock-in amplifier, DAQ: data acquisition card, i_{AC} : interferometric photo detector current, t : time, FT: Fourier transform, ℓ : geometrical optical path length in the sample, λ : wavelength, S : power spectrum, μ_t/μ_a : attenuation/absorption coefficient, PS: polystyrene spheres

The time dependency of ΔL in Eq. 4.3 a and b is caused by the linear translation of the mirror in the reference arm, which moves triangularly with a frequency f_R and a range ΔR , resulting in a velocity $v_R = 2f_R\Delta R$. This movement causes Doppler shifting of the reference arm field, resulting in a frequency modulation on $i_{AC}(t)$. Hence, it provides us with the relation between f and λ :

$$f = \frac{2v_R}{\lambda} = \frac{4f_R\Delta R}{\lambda} \quad (4.6)$$

The scanning range ΔR results in a roundtrip (geometrical) path length scanning window $\Delta\ell$ within the sample:

$$\Delta\ell = \frac{2\Delta R}{n_g} \quad (4.7)$$

with n_g the group refractive index of the medium. A single spectrum S is obtained from the $i_{AC}(t)$ within this scanning window (Eq. 4.5), over a time interval of $1/(2f_R)$. The axial

resolution at which \mathbf{S} is acquired ($\frac{1}{2}\Delta\ell$) is therefore $\Delta R/l_c$ times larger or ‘worse’ than the axial resolution at which $i_{AC}(t)$ can be acquired (l_c/n_g).

The spectral resolution $\Delta\lambda$ of \mathbf{S} can be derived by differentiating f to λ and by using Eq. 4.6:

$$\frac{df}{d\lambda} = -\frac{4f_R\Delta R}{\lambda^2} \Rightarrow \Delta\lambda = \left| -\frac{\lambda^2\Delta f}{4f_R\Delta R} \right| \quad (4.8)$$

In Eq. 4.8, Δf denotes the resolution in the frequency domain. Due to the time-frequency Fourier pair in Eq. 4.5 and the Nyquist criterium ($f_s < 2f$), $\Delta f = f_s/N$, with f_s the sampling frequency at which $i_{AC}(t)$ is acquired and N the number of samples. Since all N samples are acquired within one sweep of the reference mirror, $f_s = 2f_R N$ and hence, $\Delta f = 2f_R$. Substitution into Eq. 4.8 results in:

$$\Delta\lambda = \frac{\lambda^2}{2\Delta R} \quad (4.9)$$

In summary, we end up with a spectrum \mathbf{S} that is acquired over an optical path length interval $\Delta\ell$ with spectral resolution $\Delta\lambda$. The spectrum \mathbf{S} is *localized*, since $\Delta\ell$ determines the sample volume from which \mathbf{S} is acquired and the optical path length difference ΔL between the sample and reference arms determines the depth from which \mathbf{S} is acquired in the sample. Eq. 4.8 shows that a trade-off exists between the spectral and spatial resolution of \mathbf{S} . Hence, ΔR should be chosen small enough to adequately probe the sample’s spatial variation, but large enough to obtain a $\Delta\lambda$ that is sufficient to retrieve the spectral features of interest in \mathbf{S} .

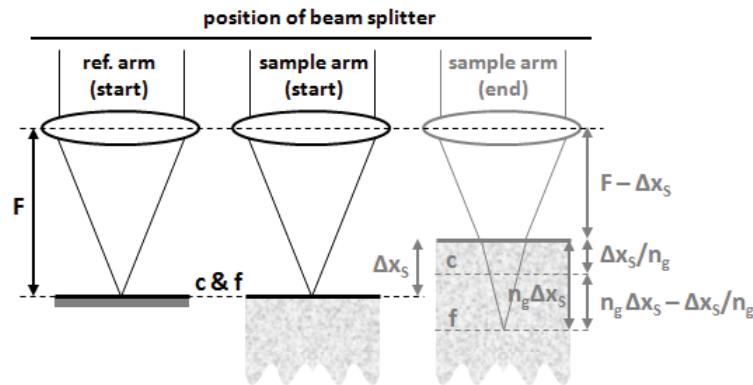


Figure 4.2 Schematic illustration of the focus tracking process. Start: the position of the coherence gate (c) and the focus (f) are matched at the sample surface. End: the sample is shifted with Δx_s towards the sample lens, which induces a mismatch between the positions of the focus and the coherence gate in the sample. Adjusting the reference arm length with $\Delta x_R = \Delta x_s(n_g^2 - 1)$ rematches the positions of the focus and the coherence gate (see text).

To determine the optical coefficients of the sample, multiple spectra \mathbf{S} are required, originating from different roundtrip geometrical path lengths ℓ (or depths $d = \ell/2$) within the sample. The geometrical path length ℓ in the sample is determined by ΔL . In this thesis, we control ΔL by varying the length of the sample arm, i.e. we displace the sample towards the sample lens with interval Δx_s , resulting in a geometrical path length shift of $\ell = 2n\Delta x_s$. Figure 4.2 illustrates the shifts in the positions of the focus ($n_g\Delta x_s$) and the location from which we acquire $i_{AC}(t)$ ($\Delta x_s/n_g$, i.e. the coherence gate) induced by a sample displacement Δx_s . In order to realign the focus with the coherence gate, we elongate the length of the reference arm with $\Delta x_R = n_g \cdot (n_g\Delta x_s - \Delta x_s/n_g) = \Delta x_s(n_g^2 - 1)$, more commonly known as ‘focus tracking’ [7].

Acquiring \mathbf{S} at multiple path lengths ℓ within the sample results in a dataset $\mathbf{S}(\ell)$ which is illustrated in Figure 4.1. When the acquired $i_{AC}(t)$ is dominated by single scattered light, \mathbf{S} decays exponentially with ℓ , which is described by Beer’s law [12]:

$$\mathbf{S}(\ell) \propto \mathbf{S}_0 \cdot e^{-\mu_t \cdot \ell} \quad (4.10)$$

in which \mathbf{S}_0 is the source power spectrum and μ_t is the attenuation coefficient of the sample, which is the sum of the absorption coefficient μ_a and scattering coefficient μ_s of the sample:

$$\mu_t = \mu_a + \mu_s \quad (4.11)$$

The values of μ_a and μ_s can be obtained by separating their individual contributions to μ_t as described in Section 4.3.2 and Chapter 6.

4.3 Materials and methods

4.3.1 System and acquisition

Our LCS system (Figure 4.1) consists of a Michelson interferometer with a low pass filtered supercontinuum light source (SC430-4, Fianium Ltd., UK). The system is optimized for a bandwidth of 455 – 680 nm, resulting in a coherence length of $\sim 1.5 \mu\text{m}$ (Eq. 4.4). The light is focused by 25 mm focal length achromatic lenses on the sample and a piezo-driven reference mirror. The reference arm power can be adjusted with a neutral density filter in the reference arm and the optical power at the sample is 2.5 mW. Both the sample and the reference mirror are mounted on motorized translation stages which are used for controlling ℓ of the light in the sample ($\ell = 0 - 2 \text{ mm}$, in steps of $27 \mu\text{m}$). Around ℓ , the signal is modulated by scanning the piezo-driven reference mirror at 23 Hz over a range of $\Delta R = 40 \mu\text{m}$. Non-linearities in reference mirror velocity are avoided by excluding the edges of the piezo sweep, resulting in an effective scanning range of $30 \mu\text{m}$ and a scanning window of $\Delta \ell \approx 44 \mu\text{m}$ within the sample (Eq. 4.7, with group refractive index $n_g = 1.35$ for aqueous solutions of polystyrene spheres, see below). Focus tracking, as described in Section 4.2, was ensured. The depth of focus of the sample arm lens is $60 \mu\text{m}$ in air.

A graded index multimode fiber ($\emptyset 62.5 \mu\text{m}$, NA=0.27, length $L = 1.1 \text{ m}$, $n_{\text{core}} \approx 1.5$, M31L01 Thorlabs, USA) guides the reflected light from both arms to a photodiode

(2001, New Focus, USA). Multimode detection sacrifices spatial resolution compared to single mode detection, but makes the system less sensitive to changes in sample geometry that affect the spectral bandwidth of the light coupled into the detection fiber. A schematic overview of the signal processing after acquisition is given in Figure 4.1. The time signal is band pass filtered by the photodiode (1-10 kHz) and demodulated by a lock-in amplifier at the spectral center frequency of 6690 Hz with a low pass frequency of 5 kHz, corresponding to a center wavelength of 550 nm and a bandwidth of 410 nm. Per scanning window, 512 samples of amplitude and phase are digitized by a 12-bit data acquisition card (USB-6009, National Instruments, USA) and multiplied by a Hanning window before applying a Fourier transform to obtain $S(\ell)$ (Eq. 4.5). The frequency axis f of the Fourier spectrum is converted to wavelength using Eq. 4.6, with $v_R = 1.84$ mm/s. Correct wavelength mapping of the spectra was verified using two narrow band pass filters at wavelengths of 510 and 577 nm. For the scanning window $\Delta\ell$ of 44 μm , the spectral resolution is $\Delta\lambda \approx 8$ nm at 680 nm (Eq. 4.9).

For each geometrical path length ℓ , the average of 400 measured spectra $S(\ell)$ is binned into wavelength regions of 8 nm to obtain equidistant data points for $S(\ell)$. Attenuation coefficients per wavelength region μ_t are determined by fitting Eq. 4.10 to $S(\ell)$ vs. ℓ (from $\ell = 80$ to 2000 μm), using a nonlinear least squares fitting algorithm. The accuracy in μ_t is quantified by the 95% confidence intervals (c.i.) of the fitted μ_t [5]. The signal to noise ratio (SNR) was 112 dB, measured on the time signal of the reflection from a mirror in the sample arm, which was attenuated by a 3.0 optical density filter.

4.3.2 Samples

We prepared two sets of samples with three different concentrations of scattering polystyrene spheres (20%, 10% and 5% dilutions from a stock of 25 mg/ml, 392 nm diameter, KI-PPS-0.4, G. Kisker GbR, Germany). Mie calculations gave an anisotropy of $g = 0.78$ and scattering coefficients of 10.9 mm^{-1} , 5.5 mm^{-1} and 2.7 mm^{-1} at the center wavelength. The first set contained only the three concentrations of polystyrene spheres; the second set contained the same concentrations of polystyrene spheres as the previous set, but also a fixed concentration of absorbing green dye (37.5% Ecoline #600, Royal Talens, The Netherlands).

The attenuation coefficient is the sum of the scattering and absorption coefficients μ_s and μ_a of the sample (Eq. 4.11). A straightforward method to derive the μ_a from the samples with dye, is by subtracting μ_s from the measured μ_t . Hence, for each sample pair (absorbing/non-absorbing) with identical concentration of polystyrene spheres (i.e. identical μ_s), we subtracted the μ_t of the non-absorbing sample from the μ_t of the absorbing sample (Figure 4.1).

An absorption spectrum of the dye only was determined in a separate transmission measurement by a spectrograph (USB4000, Ocean Optics, USA) for validation of the measured μ_a . Since Brownian motion of the polystyrene spheres causes Doppler broadening of the LCS spectra, we equally broadened the μ_a transmission spectrum to enable adequate comparison between the two. The average Doppler frequency shift Δf_D induced by the Brownian motion of a sphere with radius r is given by $(4k_B \cdot T \cdot n^2)/(3\eta \cdot r \cdot \lambda^2)$, with k_B the Boltzmann constant ($\text{m}^2 \cdot \text{kg} \cdot \text{s}^{-2} \cdot \text{K}^{-1}$), T the temperature (K), n the refractive index of the medium and η the viscosity of the medium ($\text{kg} \cdot \text{m}^{-1} \cdot \text{s}^{-1}$) [4,13]. For the

polystyrene spheres in this Chapter, $\Delta f_D = 167$ Hz, which corresponds to a wavelength broadening of 14 nm around the center wavelength of 550 nm. Hence, broadening of the μ_a transmission spectrum was achieved by convolution with a Lorentzian with a line width of 14 nm [4,13].

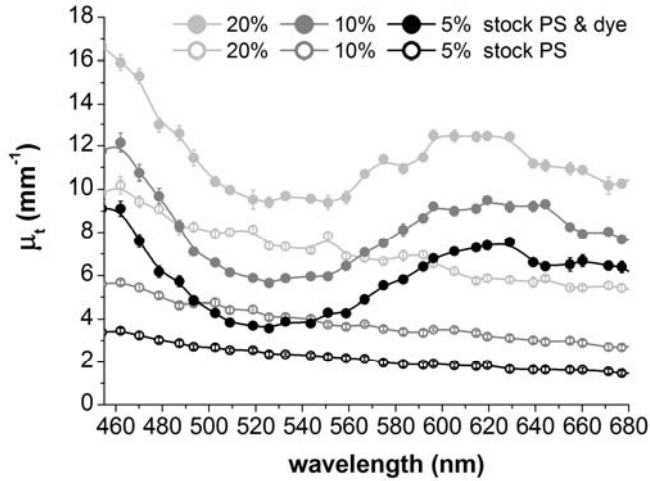


Figure 4.3 Attenuation spectra for three concentrations of polystyrene spheres (PS) with and without dye. Error bars represent the 95% c.i. of the fitted values. The lines through the data points are drawn as a guide to the eye.

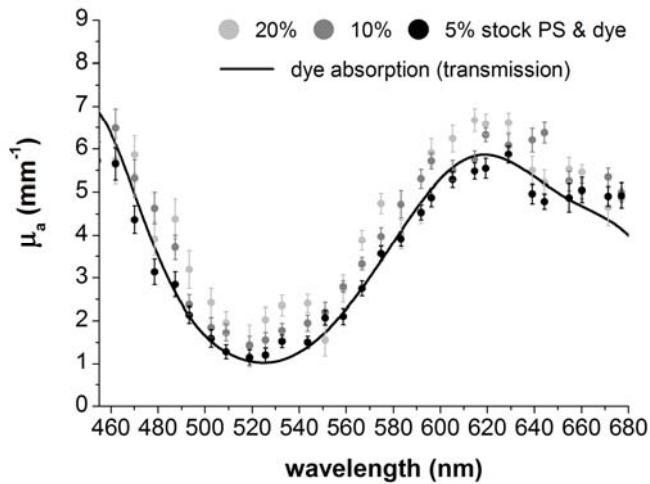


Figure 4.4 Absorption spectra for three samples with varying concentrations of polystyrene spheres (PS), but constant concentration of absorbing dye. Error bars represent the 95% c.i. of the fitted values.

4.4 Results

The measured attenuation spectra of the six samples are shown in Figure 4.3. The determined attenuation coefficients demonstrate the feasibility of LCS to extract the μ_t with an accuracy of $\pm 0.25 \text{ mm}^{-1}$. For the non-absorbing samples (only polystyrene spheres), the μ_t scale linearly with the concentration and all lie within the range of scattering coefficients of tissues [14].

The absorption spectra of the green dye derived from the three pairs of scattering samples are shown in Figure 4.4. Due to error propagation of the 95% c.i. in the subtraction, the accuracy for μ_a is approximately twice the accuracy of the μ_t determination ($\pm 0.5 \text{ mm}^{-1}$). The three spectra overlap within 2 mm^{-1} , which suggests that our method of determining μ_a holds for a broad range of scattering coefficients. Furthermore, the spectra show good agreement within 1.5 mm^{-1} with μ_a of the dye only (Figure 4.4, solid line).

4.5 Discussion and conclusion

In the preceding analysis of μ_a we assumed that the LCS signal from the non-absorbing samples decays exponentially with $\mu_s \times \ell$. Because our detection geometry may not be optimized to reject multiple scattered light (weak confocality because of low NA optics and the multimode detection fiber), the observed decay with ℓ can be shallower than predicted by μ_s . The separation of μ_s and μ_a by the subtraction of μ_t from a non-absorbing sample can still be applied, because absorption takes place along the photon's controlled path and therefore attenuates according to Beer's law [4,15].

The wavelength dependence of the sample's phase refractive index causes dispersion of the time signal, which leads to an increase of the axial resolution for large path lengths inside the sample. Correct acquisition of \mathbf{S} requires that the dispersed time signal is still sampled within our scanning window, i.e. the axial resolution ($l_c/n_g \approx 1.1 \text{ }\mu\text{m}$) at which we acquire $i_{AC}(t)$ is smaller than the axial resolution ($\frac{1}{2}\Delta\ell$) at which we acquire \mathbf{S} (Section 4.2). According to Hizenberger *et al* [16], the broadened axial resolution at a depth d in the sample is given by:

$$\frac{l_{c,\text{dispersed}}}{n_g} = \frac{1}{n_g} \sqrt{l_c^2 + (GD \cdot d \cdot \lambda_{FWHM})^2} \quad (4.12)$$

with GD the group dispersion of the sample. GD is determined by the second derivative of the phase refractive index of the sample [17]: $GD = -\lambda_0 \cdot (d^2n/d\lambda^2)$. For our system, this leads to an increase of the axial resolution of $i_{AC}(t)$ from $1.1 \text{ }\mu\text{m}$ to $8 \text{ }\mu\text{m}$ when the path length is set at 2 mm ($d = 1 \text{ mm}$). Since the dispersed $i_{AC}(t)$ will still be sampled within the axial resolution of \mathbf{S} ($22 \text{ }\mu\text{m}$), sample dispersion will not affect the power spectrum and hence, our calculation of μ_t .

Besides sample dispersion, intermodal dispersion may occur between the modes that are guided through the multimode detection fiber. The maximum number of modes M that can be guided through our multimode detection fiber is ~ 2300 , since $M \approx (\pi \cdot r \cdot NA / \lambda_0)^2$, with r the radius and NA the numerical aperture of the fiber [18]. The

modal dispersion between the first and the last mode is given by $L \cdot (NA/n_{\text{core}})^4 / 16 \approx 70 \mu\text{m}$ for our system [18], resulting in a dispersion of $70/M \approx 0.03 \mu\text{m}$ between two subsequent modes. Hence, the majority of elongated path lengths due to intermodal interference is sampled within our scanning window of $44 \mu\text{m}$ and we speculate that this effect has no substantial influence on our calculation of μ_t . In addition, we compared the system performance using a multimode detection fiber to the performance using a single mode detection fiber. This comparison gave no substantial difference in dynamic range and outcome of the μ_t measurement, indicating that modal dispersion and intermodal interference have no significant effect on our measurements.

The current accuracy of $\pm 0.5 \text{ mm}^{-1}$ of our determination of μ_a will be sufficient to measure biological variation in absorption, e.g. a 6% oxygenation change or a 2% change in hemoglobin concentration in whole blood in our wavelength range [14]. However, the variation in the absorption spectra in Figure 4.4 suggest that the accuracy may be worse than predicted by the 95% c.i.. Thus to improve the clinical value, the accuracy must be improved. Furthermore, obtaining a reference spectrum may be challenging *in vivo*, but alternative methods to separate scattering and absorption from a single attenuation profile have been proposed [2,6].

Whereas in this Chapter μ_a is measured in non-layered, homogeneous samples, LCS has potential to measure μ_a in individual layers of layered media such as human skin. The controlled path length and the confined measurement volume due to the confocality of the system, in principle allow to measure within a layer of choice. In complex media, where more than one chromophore contributes to the measured μ_a , methods such as multivariate analysis [1] are required to obtain the contribution of each individual chromophore.

In conclusion, we present absorption spectra from back scattered signals of polystyrene sphere solutions with green absorbing dye, with μ_s and μ_a within the physiological range of tissue. Our method applies for a broad range of scattering coefficients and agrees with transmission spectroscopy. Compared to other spectroscopic techniques, LCS controls the path length of the detected light inside a sample, which enables both quantitative and potentially localized measurements of absorption coefficients. Since absorption coefficients are directly related to chromophore concentrations, LCS is a promising technique for *in vivo* determination of tissue chromophore concentrations in individual tissue layers.

References

1. P. Rolfe, "In vivo near-infrared spectroscopy", *Annual Review of Biomedical Engineering* **2**, 715-754 (2000)
2. M.G. Nichols, E.L. Hull, T.H. Foster, "Design and testing of a white-light, steady state diffuse reflectance spectrometer for determination of optical properties of highly scattering media", *Applied Optics* **36**, 93-104 (1997)
3. Amelink, H.J.C.M. Sterenborg, M.P.L. Bard, S.A. Burgers, "In vivo measurement of the local optical properties of tissue by use of differential path-length spectroscopy", *Optics Letters* **29**, 1087-1089 (2004)
4. Varghese, V. Rajan, T.G. van Leeuwen, W. Steenbergen, "Path length resolved measurements of multiple scattered photons in static and dynamic turbid media using phase modulated low coherence interferometry", *Journal of Biomedical Optics* **12**, 024020 (2007)

5. D.J. Faber, T.G. van Leeuwen, "Are quantitative attenuation measurements of blood by optical coherence tomography feasible?", *Optics Letters* **34**, 1435-1437 (2009)
6. C. Xu, D.L. Marks, M.N. Do, S.A. Boppart, "Separation of absorption and scattering profiles in spectroscopic optical coherence tomography using a least-squares algorithm", *Optics Express* **12**, 4790-4803 (2004)
7. B. Hermann, K. Bizheva, A. Unterhuber, B. Povazay, H. Sattman, L. Schmetterer, A.F. Fercher, W. Drexler, "Precision of extracting absorption profiles from weakly scattering media with spectroscopic time-domain optical coherence tomography", *Optics Express* **12**, 1677-1688 (2004)
8. A. Dubois, J. Moreau, C. Boccara, "Spectroscopic ultrahigh-resolution full-field optical coherence microscopy", *Optics Express* **16**, 17082-17091 (2008)
9. D.T. Delpy, M. Cope, P. van der Zee, S. Arridge, S. Wray, J. Wyatt, "Estimation of optical pathlength through tissue from direct time of flight measurement", *Physics in Medicine and Biology* **33**, 1433-1442 (1988)
10. T.H. Pham, O. Coquoz, J.B. Fishkin, E. Anderson, B.J. Tromberg, "Broad bandwidth frequency domain instrument for quantitative tissue optical spectroscopy", *Review of Scientific Instruments* **71**, 2500-2513 (2000)
11. J.A. Izatt, M.A. Choma, "Theory of Optical Coherence Tomography", Chapter 2 in *Optical Coherence Tomography – Technology and Applications*, W. Drexler, J.G. Fujimoto, Eds., pp. 47-72 (Springer-Verlag, 2008)
12. J.M. Schmitt, A. Knüttel, R.F. Bonner, "Measurement of optical properties of biological tissues by low-coherence reflectometry", *Appl. Opt.* **32**, 6032-6042 (1993)
13. D.A. Boas, K.K. Bizheva, A.M. Siegel, "Using dynamic low-coherence interferometry to image Brownian motion within highly scattering media", *Optics Letters* **5**, 319-321 (1998)
14. A.J. Welch, M.J.C. van Gemert, "Optical-thermal response of laser-irradiated tissue" (Plenum Press, 1995)
15. A.L. Petoukhova, W. Steenbergen, T.G. van Leeuwen, F.F.M. de Mul, "Effects of absorption on coherence domain path length resolved dynamic light scattering in the diffuse regime", *Applied Physics Letters* **81**, 595-597 (2002)
16. C.K. Hitzengerger, A. Baumgartner, W. Drexler, A.F. Fercher, "Dispersion effects in partial coherence interferometry: implications for intraocular ranging", *Journal of Biomedical Optics*, **4**, 144-151 (1999)
17. M. Daimon, A. Masumura, "Measurement of the refractive index of distilled water from the near-infrared region to the ultraviolet region", *Applied Optics* **46**, 3811-3820 (2007)
18. B.E.A. Saleh, M.C. Teich, "Fiber Optics", Chapter 8 in *Fundamentals of Photonics*, pp. 272-309 (Wiley-Interscience, 1991)